Plasmonically Enhanced Thin-Film Amorphous Silicon Solar Cells

T. Sonsalla and S. Zivanovic

Institute for Micromanufacturing
Louisiana Tech University, Ruston, LA, USA, sz@latech.edu

ABSTRACT

Due to the atomic structure of hydrogenated amorphous silicon (a-Si:H), power conversion efficiencies (PCE) are much lower than in crystalline silicon counterparts. In order to increase PCE of a-Si:H solar cells, this study focused on incorporating metal nanoparticles onto the front transparent conductive electrode to induce increased forward light scattering and near-field light coupling.

Different deposition thicknesses and annealing temperatures were used to analyze the effects on metal nanoparticle size and coverage. It was discovered that initial deposition thickness is linearly related to metal nanoparticle size. Furthermore, annealing the 5-15 nm silver samples at 300°C led to a Ag nanoparticle coverage of 30% regardless of initial Ag deposition thickness. Deposition of Ag layers of 7.4 nm and 10 nm in the glass/ITO/Ag/PIN a-Si:H/ITO/Al solar cells achieved the best PCEs. Thus, future investigation into Ag deposition thicknesses between 7.4-10 nm should be performed.

Keywords: solar cells, surface plasmons, metal nanoparticles, amorphous silicon, plasmonics

1 INTRODUCTION

Hydrogenated amorphous silicon (a-Si:H) can absorb the visible part of the solar spectrum better than crystalline silicon. For this reason, a-Si:H solar cells can be much thinner than crystalline silicon solar cells. Thinner cells reduce fabrication costs by utilizing less silicon. However, due to the atomic structure of amorphous silicon, power conversion efficiencies are much lower than in crystalline silicon counterparts.

There are three ways metal nanoparticles have been utilized to improve solar cell efficiency: on the front of the transparent conducting electrode to promote light scattering [1], metal nanoparticles within the semiconductor material that act as subwavelength antennas [1, 2], and at back of the semiconductor coupling sunlight into SP modes at the metal/semiconductor interface [1]. For this reason, this study aims to improve glass/ITO/PIN a-Si:H/ITO/Al solar cell power conversion efficiency (PCE) via inclusion of a metal nanoparticle layer between the ITO/PIN a-Si:H layers.

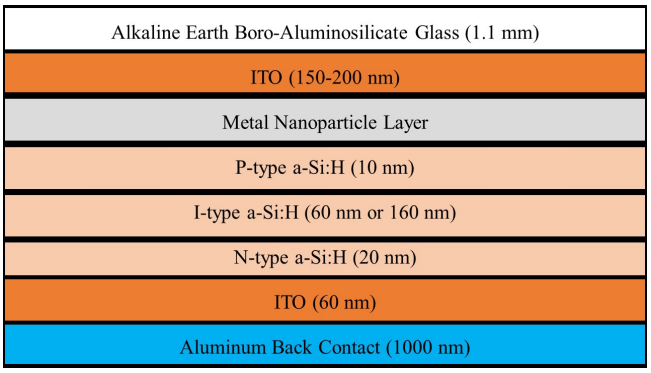

Figure 1: Solar cell structure.

2 EXPERIMENTAL

2.1 Solar Cell Structure

This study investigated solar cell structures of glass/ITO/metal nanoparticles/a-Si:H/ITO/Al and the structure is shown in Figure 1. Delta Technologies Corning glass substrates coated with an ITO thickness of 150-200 nm and sheet resistance of 4-10 Ω/□ made up the glass/ITO layer. The a-Si:H structure was a PIN structure with p-type thickness of 10 nm, i-type thicknesses of 60 (run 1) and 160 nm (run 2), and n-type thickness of 20 nm grown by FEThinFilms LLC, Centennial, CO. The ITO layer between the a-Si:H and Al layer was 60 nm. The aluminum back electrode thickness was 1000 nm.

2.2 Metal Nanoparticle Fabrication

Metal nanoparticle were e-beam evaporated by a CHA Mark 50 (substrates deposited in cleanroom at Georgia Tech University) and a CHA BEC-600-RAP (substrates deposited in cleanroom at Louisiana Tech University).

Annealing was preformed on a hot plate in a nitrogen hood (specific to silver samples), and in a Vulcan furnace (used to obtain temperatures greater than 300°C). Annealing temperature was determined by testing multiple temperatures, and selecting the temperature that produced the highest average optical transmittance.

2.3 Sheet Resistance Measurement

A Lakeshore 75013 SCSM Hall Measurement System was used to measure the sheet resistance of the samples.

2.4 Scanning Electron Microscope Image Collection and Nanoparticle Measurement

A Hitachi S-4800 cold-cathode field emmission scanning electron microscope (FE-SEM) was used to image all sample surfaces. Samples were imaged before any manipulation, after e-beam evaporation, and after thermal annealing. Calculation of nanoparticle size and coverage was found by uploading SEM images into ImageJ software. The software outlined nanoparticles via image manipulation and output areas of individual nanoparticles. The areas of the individual nanoparticles were converted to diameters using Eq. 1.

$$Diameter = \sqrt{\frac{Area}{\pi}} * 2 \quad (1)$$

2.5 Transmittance, Reflectance, and Absorbance Measurement

A Filmetrics F10-RT spectral reflectometer was used to measure optical reflectance and transmittance of the ITO samples. Absorbance was calculated using Eq. 2.

$$Absorbance = 1 - Transmittance - Reflectance \quad (2)$$

2.6 Solar Cell Fabrication and Testing

The PIN a-Si:H active layer of the solar cell was done by FEThinFilms, LLC in Centennial, CO using PECVD.

A Spectra Physics 66907 solar simulator was used for solar cell testing and output an Air Mass 1.5 Global Reference spectrum. A Newport 91150V Reference Cell and Meter were utilized to measure the amount of optical power from the solar simulator.

3 RESULTS AND DISCUSSION

3.1 Sheet Resistance Results

Figure 2 shows measured sheet resistances of Delta Technologies CB-40IN ITO coated glass substrates before and after silver deposition. The sheet resistance of the CB-40IN samples before any substrate manipulation was approximately 7.48 Ω/□. The substrate sheet resistance did not change after deposition of 1 nm and 5 nm of silver. However, deposition of 10 nm of silver caused a reduction in sheet resistance to 5 Ω/□, while 15 nm of silver reduced sheet resistance to 2.92 Ω/□. The lack of change in sheet resistance after 1 nm and 5 nm silver deposition suggested that percolation was not reached. However, at a deposition thickness of 10 nm a reduction in sheet resistance occurred. Thus, the percolation threshold must be between 5 nm and 10 nm.

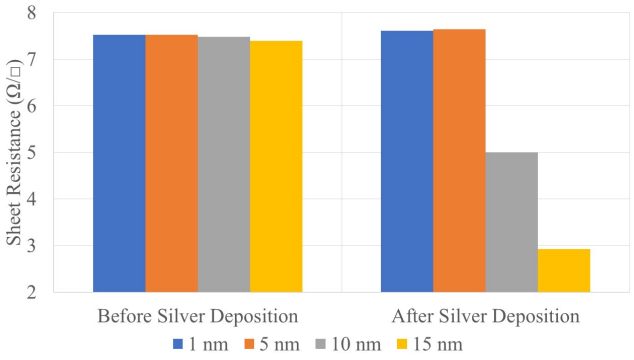

Figure 2: Sheet resistance comparison of substrates deposited with 1 nm, 5 nm, 10 nm, and 15 nm of silver.

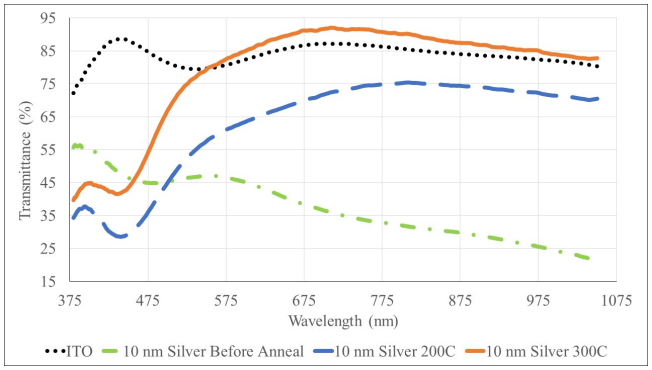

Figure 3: Comparison of the transmittance spectrums of 10 nm silver substrates after e-beam evaporation (dash dot green line) and after annealing at different temperatures (200°C-long dash blue line and 300°C-solid red line) and unmodified ITO coated glass substrate (dotted black line).

3.2 Annealing Temperature Results

Different annealing temperatures were utilized for each metal. The annealing temperature for a particular metal was selected if it produced the maximum average transmittance. The best annealing temperature was then used to anneal different deposition thicknesses.

Transmittance in the wavelength region of 390-700 nm is important for a transparent conductive electrode (TCE) designed for an amorphous silicon solar cell because this is the region where amorphous silicon is able to convert light to an electron-hole pair due to its energy bandgap of 1.8 eV.

Figure 3 compares the transmittance spectrum of an unmodified ITO coated glass substrate, ITO coated glass substrate after deposition of 10 nm of silver, and two substrates coated with 10 nm of silver annealed at two different temperatures. The increase in transmittance when annealing at a higher temperature was most likely due to better coalescence of the metal ma-

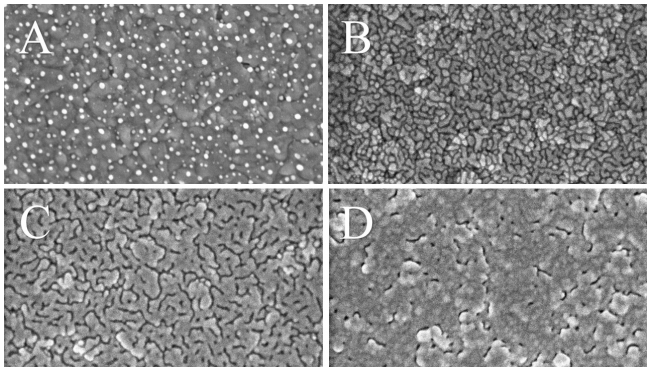

Figure 4: SEM images of CB-40IN sample surface after (A) 1 nm (B) 5 nm (C) 10 nm (D) 15 nm silver e-beam evaporation.

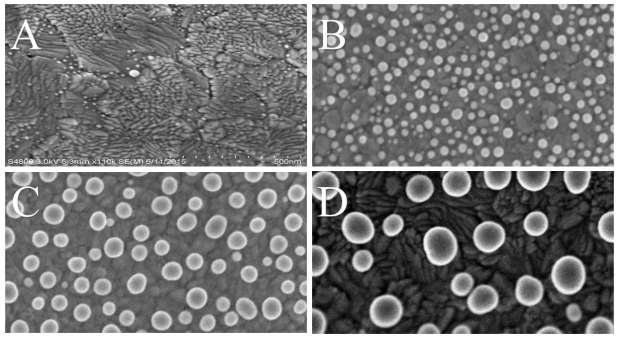

Figure 5: SEM images of CB-40IN sample surface after (A) 1 nm (B) 5 nm (C) 10 nm (D) 15 nm silver e-beam evaporation and 1 hour 300 °C annealing.

terial into nanoparticles. Furthermore, the distribution of nanoparticles may have become more periodic with the higher annealing temperature, which could lead to better scattering characteristics (i.e. improving transmittance).

3.3 SEM Results

Figure 4 shows SEM images of the substrates deposited with 1 nm, 5 nm, 10 nm, and 15 nm of silver. Figure 5 shows SEM images of the substrates deposited with 1 nm, 5 nm, 10 nm, and 15 nm of silver and annealed for 1 hour at 300°C. The nanoparticle coverages for the 1 nm, 5 nm, 10 nm, and 15 nm samples were 4.70%, 32.8%, 29.3%, and 30.3%. The average particle diameters for the 1 nm, 5 nm, 10 nm and 15 nm substrates were 4.0 nm, 30.2 nm, 70.3 nm, and 118 nm, respectively.

Previous studies have shown the ideal nanoparticle coverage for solar cells is around 10% [3, 4]. However, none of these samples met this ideal coverage after annealing. The 1 nm sample before annealing had a particle coverage close to 10%, but after annealing particle coverage was reduced. This could be due to a lack of metal material available on the ITO surface. The 1 nm substrate was the only substrate to not require annealing to have nanoparticles present. It can be concluded that increasing deposition thickness led to an increase in maximum, average, and minimum particle diameter. The increase in particle size led to a localized surface plasmon resonance that was broader and redshifted. Furthermore, it can be concluded that nanoparticle coverage did not change with deposition thickness over 5 nm. For this reason, it can be assumed increasing the deposition thickness would create larger particles, but there would be fewer of them to keep the nanoparticle coverage around 30%. It could have been beneficial to investigate whether nanoparticle coverage could be controlled with a template placed over the substrate during deposition. Additionally, it may have been beneficial to monitor the mass of the substrates during processing to further understand the metal nanoparticle formation dynamics.

3.4 Transmittance, Reflectance, and Absorbance Results

The 1 nm sample had the highest transmittance of the non-annealed samples. Additionally, the transmittance of the 1 nm sample in the 390-700 nm visible wavelength range is higher than all other samples. Furthermore, the 1 nm sample had a surface plasmon resonance at 481 nm (i.e. absorbance peak), whereas the other samples had no distinct absorbance peak because nanoparticles were not formed.

The 1 nm sample had the highest transmittance of the annealed samples in the 390-700 nm range. The 7.4 nm sample had the lowest transmittance in the 390-700 nm range of the annealed samples.

3.5 Solar Cell Results

Figure 6 shows current density versus voltage for the reference cell (without silver layer) and substrate 6 (with 7.4 nm silver layer between ITO/p-type a-Si:H layers) from run 2.

Shunt resistances were higher in solar cells with a thicker a-Si:H deposition thickness. Higher shunt resistances suggest better p-i-n junctions because a higher shunt resistance means there are no pinholes or cracks in the device structure to cause defect centers to arise leading to recombination. Furthermore, higher shunt resistance leads to a device that is more stable over time and has higher PCE. Shunt resistances were lower in substrates that had metal nanoparticles on the surface during PECVD deposition. Metal nanoparticles on the substrate surface may have led to them traversing the junction (due to device thickness of 90 nm), which would

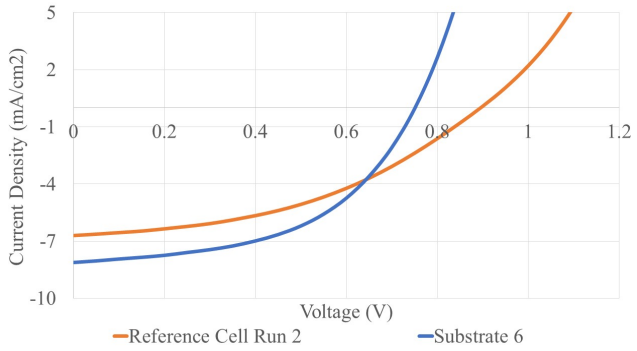

Figure 6: Comparison of reference cell (run 2) and substrate 6 (run 2) current density-voltage curves.

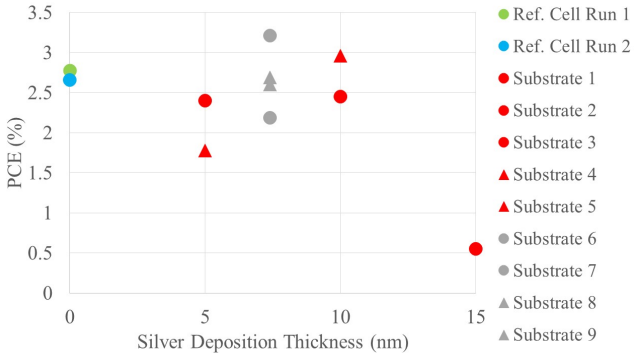

Figure 7: Power conversion efficiency (PCE) versus Ag deposition thickness with run 1 cells are in red and run 2 cells are in gray. Run 1 reference cell is in green and run 2 reference cell is in blue. Annealed substrates are circles, while non-annealed substrates are triangles.

lower shunt resistance as it would create defect centers within the device.

Series resistance of the non-annealed substrates appeared to decrease with an increase in metal deposition thickness. This was expected because sheet resistance equals resistivity divided by thickness. However, the series resistance of the annealed substrates increased with an increase in deposition thickness. This is most likely due to creation of a larger electrical interface due to metal nanoparticles on the substrate surface.

Substrates that outperformed the reference cells typically had higher short circuit densities (see Fig. 6). This suggests the substrates had better optical properties than the reference cell to produce higher PCEs. Figure 7 shows the power conversion efficiency versus metal deposition thickness for runs 1 (in red) and 2 (in gray) with annealed substrates as circles and non-annealed substrates as triangles. Silver deposition thicknesses of 7.4 nm and 10 nm produced the best PCEs. This could be due to surface plasmon polaritons (non-annealed substrates) and surface plasmons (annealed substrates) existing at the metal-amorphous silicon interface [5], which may have led to enhanced light absorption and electron-hole pair creation in the intrinsic layer. This effect coupled with the low series resistances of the substrates deposited with metal most likely led to higher PCEs.

The intrinsic a-Si:H layer thickness of 160 nm provided more working devices. However, this could be attributed to the reduction in handling of the substrates utilized in amorphous silicon deposition. Utilization of different metals (i.e. gold and aluminum) showed that silver was the only metal to cause an efficiency enhancement over the reference sample.

4 CONCLUSIONS

Electron-beam evaporation of metal onto an ITO coated glass substrate caused a reduction in sheet resistance with an increase in deposition thickness. Additionally, annealed substrates had higher light transmittance than non-annealed samples. Silver deposition thicknesses of 7.4 nm and 10 nm produced the best PCEs. These silver deposition thicknesses with and without annealing produced the highest PCEs at 2.96% (10 nm) and 3.21% (7.4 nm). However, different silver deposition thicknesses between 7.4-10 nm should be further investigated. In conclusion, this study showed the incorporation of metal on the transparent conductive oxide of the transparent conductive electrode produced a PCE enhancement over reference cells fabricated in the same amorphous silicon deposition.

ACKNOWLEDGEMENTS

This work was funded by NASA STTR grant NNX14CS11C. The authors thank the Institute for Micromanufacturing staff and Dr. Feng Zhu, FEThinFilms LLC.

REFERENCES

[1] Atwater, H., and Polman, A., 2013. "Plasmonics for improved photovoltaic devices". *Nature Materials,* ***9***, pp. 205–213.

[2] Lee, J., and Peumans, P., 2010. "The origin of enhanced optical absorption in solar cells with metal nanoparticles embedded in the active layer". *Optics Express,* ***18***(10), pp. 10078–10087.

[3] Starowicz, Z., Kulesza-Matlak, G., and Lipinski, M., 2015. "Optimization studies on enhanced absorption in thin silicon solar cell by plasmonic silver nanoparticles for the front side configuration". *Plasmonics,* ***10***(6), pp. 1639–1647.

[4] Catchpole, K., and Polman, A., 2008. "Design principles for particle plasmon enhanced solar cells". *Applied Physics Letters,* ***93***.

[5] D. Genov, V. Shalaev, A. S., 2005. "Surface plasmon excitation and correlation-induced localization-delocalization transition in semicontinuous metal films". *Physical Review B,* ***72***(113102).